An Ultrahigh Narrowband Absorber Close to the Information Communication Window

Wajid Ali
National Center for Nanoscience and Technology
Shahid Iqbal
Southeast University
Muhib Ullah
Zhejiang University
Xiaoli Wang (wangxl@nanoctr.cn)
National Center for Nanoscience and Technology https://orcid.org/0000-0003-1662-1162

Research Article

Keywords: plasmonics, absorber, sensing, metamaterial

Posted Date: July 15th, 2021

DOI: https://doi.org/10.21203/rs.3.rs-680454/v1

Version of Record: A version of this preprint was published at Plasmonics on November 2nd, 2021. See the published version at https://doi.org/10.1007/s11468-021-01557-9.

Abstract

In this paper, we demonstrate a plasmonic ultrahigh narrowband perfect absorber, which realizes an absorption intensity of up to 99.99% in the near-infrared electromagnetic spectrum regime. Different dimensional effects on absorption properties are studied using computer simulation technology (CST) with finite element method (FEM) solver. For both transverse electric (TE) and magnetic (TM) polarization, the absorber shows high stability over a wide range of incident angles. This ultrahigh absorption is attributed to synergy effect of magnetic resonance and surface plasmon resonance. Furthermore, the sensitivity goes to 300 nm/RIU for various refractive indices of different analytes. Our proposed absorber working wavelength is very close to the communication window of information, therefore, except for remarkable sensing abilities, it can also be well utilized in optoelectronic applications like optical switching, amplifiers, and all-optical plasmonic modulators.

Introduction

Metamaterials and metasurfaces are artificially patterned materials consisting of periodically arranged subwavelengths ‘meta-atoms’. The meta-atoms design and geometry flexibility have branded metamaterial as designable permittivity and permeability materials [1–4], and make them widely used in electromagnetic (EM) induced transparency (EIT) [5–7], imaging [8–10], EM waves detections [11], ultrahigh sensitive sensors [12–14], EM invisibility cloaking [15], and solar cells [16–19]. Because of the huge investment in the solar energy harvesting systems, the plasmonic and metamaterial perfect absorbers have aroused great attention in various fields of technologies. The perfect absorbers are categorized into two, the narrow- and broad- band absorbers [20], where broadband absorbers have prominent applications in ultrashort pulse generation [21], photovoltaics [22], and thermal emitters [23], and narrowband absorbers have numerous applications in nonlinear photonics like optical modulators [24], and switches [25]. Moreover, the ultra-narrow band perfect absorbers in both visible and near-infrared regions are also of great importance in refractive index sensors. Although some narrow-band absorbers have been studied [26–29], most of them have polarization or angle sensitivity or lower absorption intensity, which limit their potential applications. In this work we propose an ultrahigh narrowband absorber with absorbance up to 99.99% close to the information telecommunication window. The absorber also reveals an outstanding performance in polarization and angle independence. The sensitivity can achieve 300 nm/RIU for various refractive indices of different analytes.

Result And Discussion

The schematic representation of the tunable hybrid metasurface is shown in Fig. 1 as a three-dimensional structure diagram. The device's topmost layer is made of gold-alumina nanoring with a common air hole of radius Rin. The thicknesses of dielectric alumina Al_2O_3 and plasmonic gold is h_1 = 30 nm and h_2 = 35 nm, with inner and outer radii Rin = 65 nm and Rout = 130 nm, respectively. The bottom gold film with thickness h_3 = 150 nm is used as a ground layer to guarantee total reflection and eradicate any incident EM wave transmission. The periodicity of the unit cell of metamaterial is P = 500 nm.

Alumina's dielectric function is taken from Malitson and Dodge [30], while noble gold is obtained from P. B. Johnson and R. W. Christy [31]. The whole structure is illuminated with plane electromagnetic waves of propagation constant K directed in negative z-axis. Under the FEM solver for the Maxwell equation, here CST microwave studio is employed to simulate and study the response of planner EM waves for both TE and TM polarization at various incident angles. For the meta-atom simulation purposes, the unit cell boundary conditions are employed periodically in the x and y direction and open (add space) in the z-direction.

Evaluating the proposed hybrid metasurface's ability in both absorption A and reflection R, Fig. 1(b) gives the optical responses at normal incident of plane EM waves. The absorption intensity can reach 99.99% at 1490 nm wavelength, which is also very close to the communication window (1550 nm). In this device, the suppression of the reflectance R at normal incidence is because of the electric and magnetic dipole matching or, in other words, the matching of the impedance of the device with free space at the frequency of operation.

The meta-device ensures near-perfect absorption of the EM waves in a specific regime from zero reflectance and transmittance. Figure 2 displays the absolute values of electric and magnetic field distribution of the proposed device at normal incidence to the plane of the device. As the device has a metal-insulator-metal (MIM) configuration, therefore the Fabry Perot cavity in the alumina region has a high tendency of the field confinement (at appropriate thickness), as shown in Fig. 2(a,b). The strongly enhanced magnetic field shown in Fig. 2(c) and Fig. 2(d) gives a clear view of magnetic resonance inside the alumina spacer and at the edges of the ring hole. To ensure the best matching of the impedance, we simulated various dielectric alumina thickness 'h_1', and the results are plotted in Fig. 3(a). The results show that 30 nm thick Al_2O_3 can provide the optimal absorption results at the normal incidence of electromagnetic waves. For the spacer of a constant thickness (i.e., h_1 = 30 nm), the varied thickness of top gold nanodisk is studied from h_2 = 25 to 45 nm, and we can see 35 nm is the optimum choice for 30 nm alumina, which makes almost completely matching of the impedance and improves the absorption intensity nearly to 100%. In both cases, we can observe that as the thickness decrease of either nanostructure, there is a red shift in the absorption peaks. The thinner dielectric enhances image charge distribution on the bottom layer due to the top metallic nanostructure's plasmonic resonance. Similarly, a thinner gold layer provides more EM transmission to the cavity region, and hence the development of standing waves enhances the total absorption ability of the device.

As our device consists of the gold-alumina disk with common inner and outer radii, therefore we investigate in Fig. 3(c, d) the effect of both radii separately. From Fig. 3(c), we observe that the absorption intensity for a solid disk or ring with R_{in}=0 nm reaches 90% at resonance peak 1300 nm of the EM wave spectrum, not as good as the optimum ring resonator. This amount of absorption is high enough to be utilized in different types of applications, like sensing and imaging. To further enhance the absorption intensity, we introduce an air hole in the nanodisk to make more chances of field confinement as elucidated for different inner radius values in Fig. 3(c). As the inner radius increases, the plasmon

resonance position shifts to a higher wavelength, and the absorption intensity increases up to 99.99% at R_{in}=50 nm for R_{out}=130 nm. After 50 nm, a further increase in inner radius reduces the absorption intensity, and at 100 nm, the intensity reduces to 70%, as shown in Fig. 3(c). As for as the outer radius is concern, for constant R_{in}, the lower R_{out} gives lower absorption, but bandwidth is sharper, as shown in Fig. 3(d). The optimum value of R_{out} is 130 nm, and with the further increase, the absorption intensity decreases.

The proposed device is further investigated for the unit cell's periodicity in Fig. 4 for five different values starting from 300 nm up to 700 nm. Among this 500 nm, center-to-center separation of the periodic layer gives the optimum result of absorption. The plasmon resonance position at all periods is nearly the same with slightly different intensity of the absorption.

In various applications, whether the absorber in a broad or narrow band range, the most important property is the less sensitivity to incidence angle and the polarization of the impinging EM waves. Here we investigate the angular stability of the proposed absorbing device for a very broad range of the incidence angles (in Fig. 5) for both TE and TM polarization. Figure 5(a) represents the absorption at 1490 nm for different incidence angles when the incident waves have TE polarization, and the device is insensitive to the whole incident angles from 0° to 70°. Furthermore, there is no critical shifting of the resonance position in this wide range at all, and such property of the absorber is very suitable for biological sensing applications. Nearly the same response is observed for TM polarization, as shown in Fig. 5(b). Here the average absorption intensity is about 99.89% until 65° of the incidence angle, and after that, there is a minor decline to 97% at the same resonance wavelength. Thus, the absorber overall response in both TE and TM polarization at a broad range of the incidence angle is nearly independent. Because of such high absorption and tunability, this proposed configuration is highly recommended for many optical applications, especially for refractive index ultrahigh sensitivity.

Finally, we are going to discuss the refractive index sensing ability of our ultrahigh plasmonic metamaterial absorber. The analytes here used with different refractive indices represent different concentrations of the glucose solution. Figure 5(c, d) displays the proposed metamaterial structure's sensing ability for various refractive indices from 1.302 to 1.352, and water is considered as a reference medium. As the refractive index changes a little bit, there is a very clear red shift in the absorption spectra's resonance peaks with no critical change in its intensity, as shown in Fig. 5(c) and Fig. 5(d). Maximum absorption achieved is 99.82%, 99.81%, 99.80%, 99.79%, and 99.77% at the resonance wavelength 1549 nm, 1552 nm, 1554 nm, 1556 nm, and 1559 nm for 1.302–1.352 broad range of the refractive indices of analytes. The analysis of the resonant wavelength versus the refractive index in Fig. 6(a) gives a straight line, which indicates that there is no critical change in the absorption intensity and the plasmon resonance of the nanostructure is highly sensitive to the change in the surrounding medium. Sensitivity S_n of refractive index based sensor can be calculated by using the following relations between wavelength resonance shift $\Delta\lambda$ and refractive index Δn

$$S_n = \Delta\lambda/\Delta n$$

The sensitivity of our proposed structure reached 300 nm/RIU, as shown in Fig. 6(b). We observe that the proposed device has a high sensitivity for very low refractive index values and high linearity in sensing. It is not far from practical realization and implementation due to the advanced electron beam lithographic technologies. Furthermore, our proposed absorber is insensitive to the angle of incidence and polarization. Therefore, it has advantages over a prism-based sensor whose work is good only at oblique incidence.

Conclusion

In summary, we proposed and theoretically designed a perfect metamaterial absorber whose absorption intensity reaches 99.99% in the near-infrared range. The ultrahigh absorption of the device is attributed to the plasmon resonance of the plasmonic nanostructure and magnetic resonance at the spacer alumina region. The device geometrical effects have been investigated for various dimensions and found the optimum thicknesses, periodicity, and inner and outer radii at which ultrahigh absorption can achevied. Furthermore, the absorber ability at both TE and TM polarization was also evaluated at a very long range of the incidence angles and found no critical change in absorption intensity as well as the plasmon resonance position. Finally, the device is tested for the sensing property for analytes with different refractive indices, and get the sensitivity of the system reached 300 nm/RIU. The proposed plasmonic device can also be utilized in the hot electron-based plasmonic modulators and switches because of the narrow perfect absorption close to the information's communication window.

Declarations

Funding: The National Natural Science Foundation of China (21975060, X.W.) and Youth Innovation Promotion Association CAS (2019039, X.W.) supported this work. W. Ali is grateful for the CAS-TWAS president fellowship.

Conflicts of interest: The authors declare no conflicts of interest.

Availability of data and material: Data underlying the results presented in this paper are not publicly available at this time but may be obtained from the authors upon reasonable request.

Code availability: The data that support the findings of this study are available from the corresponding author upon reasonable request.

Authors' contributions: X. W. conceived this research. A. W., S. I., and M. U. participated in the design and preparation of the data. All the authors read and aproved the final manuscript.

Ethics Approval: Not applicable (This work does not involve human subjects and/or animals).

Consent to participate: Informed consent was obtained from all individual participants included in the study.

Consent for publication: The participant has consented to the submission of the case report to the journal.

References

1. Landy NI, Sajuyigbe S, Mock JJ, Smith DR, Padilla WJ (2008) Perfect metamaterial absorber. Phys Rev Lett 100:207402
2. Tao H, Bingham C, Pilon D, Fan K, Strikwerda A, Shrekenhamer D, Padilla W, Zhang X, Averitt R (2010) A dual band terahertz metamaterial absorber. J Phys D Appl Phys 43:225102
3. Tao H, Landy NI, Bingham CM, Zhang X, Averitt RD, Padilla WJ (2008) "A metamaterial absorber for the terahertz regime: design, fabrication and characterization". Opt Express 16:7181–7188
4. Grant J, Ma Y, Saha S, Khalid A, Cumming DR (2011) "Polarization insensitive, broadband terahertz metamaterial absorber". Opt Lett 36:3476–3478
5. Zhang S, Genov DA, Wang Y, Liu M, Zhang X (2008) Plasmon-induced transparency in metamaterials. Phys Rev Lett 101:047401
6. Gu J, Singh R, Liu X, Zhang X, Ma Y, Zhang S, Maier SA, Tian Z, Azad AK, Chen H-T (2012) Active control of electromagnetically induced transparency analogue in terahertz metamaterials. Nat Commun 3:1–6
7. Liu N, Weiss T, Mesch M, Langguth L, Eigenthaler U, Hirscher M, Sonnichsen C, Giessen H (2010) Planar metamaterial analogue of electromagnetically induced transparency for plasmonic sensing. Nano Lett 10:1103–1107
8. Watts CM, Shrekenhamer D, Montoya J, Lipworth G, Hunt J, Sleasman T, Krishna S, Smith DR, Padilla WJ (2014) Terahertz compressive imaging with metamaterial spatial light modulators. Nat Photonics 8:605–609
9. Zhu J, Christensen J, Jung J, Martin-Moreno L, Yin X, Fok L, Zhang X, Garcia-Vidal F (2011) A holey-structured metamaterial for acoustic deep-subwavelength imaging. Nat Phys 7:52–55
10. Craster RV, Guenneau S (2012) Acoustic metamaterials: Negative refraction, imaging, lensing and cloaking. Springer Science & Business Media
11. Park S, Hong J, Choi S, Kim H, Park W, Han S, Park J, Lee S, Kim D, Ahn Y (2014) Detection of microorganisms using terahertz metamaterials. Sci Rep 4:1–7
12. Chen X, Fan W (2017) Ultrasensitive terahertz metamaterial sensor based on spoof surface plasmon. Sci Rep 7:1–8
13. He X, Zhang Q, Lu G, Ying G, Wu F, Jiang J (2016) Tunable ultrasensitive terahertz sensor based on complementary graphene metamaterials. RSCAdv 6:52212–52218
14. Wang W, Yan F, Tan S, Zhou H, Hou Y (2017) Ultrasensitive terahertz metamaterial sensor based on vertical split ring resonators. Photonics Res 5:571–577
15. Dash R, Sahu S, Mishra C, Sethi K, Palai G, Sahu S (2016) Realization of ‘non-linear invisibility cloak’using meta-material. Optik 127:9635–9639

16. Rufangura P, Sabah C (2016) Wide-band polarization independent perfect metamaterial absorber based on concentric rings topology for solar cells application. J Alloys Compd 680:473–479
17. Wang Y, Sun T, Paudel T, Zhang Y, Ren Z, Kempa K (2012) Metamaterial-plasmonic absorber structure for high efficiency amorphous silicon solar cells. Nano Lett 12:440–445
18. Kim K, Lee S (2019) Detailed balance analysis of plasmonic metamaterial perovskite solar cells. Opt Express 27:A1241–A1260
19. Wu C, Neuner B III, John J, Milder A, Zollars B, Savoy S, Shvets G (2012) Metamaterial-based integrated plasmonic absorber/emitter for solar thermo-photovoltaic systems. J Opt 14:024005
20. Lei L, Li S, Huang H, Tao K, Xu P (2018) Ultra-broadband absorber from visible to near-infrared using plasmonic metamaterial. Opt Express 26:5686–5693
21. Sotor J, Sobon G, Macherzynski W, Paletko P, Abramski KM (2015) Black phosphorus saturable absorber for ultrashort pulse generation. Appl Phys Lett 107:051108
22. Choi M, Kang G, Shin D, Barange N, Lee C-W, Ko D-H, Kim K (2016) Lithography-free broadband ultrathin-film absorbers with gap-plasmon resonance for organic photovoltaics. ACS Appl Mater Interfaces 8:12997–13008
23. Argyropoulos C, Le KQ, Mattiucci N, D'Aguanno G, Alu A (2013) Broadband absorbers and selective emitters based on plasmonic Brewster metasurfaces. Phys Rev B 87:205112
24. Sun Z, Martinez A, Wang F (2016) Optical modulators with 2D layered materials. Nat Photonics 10:227–238
25. Chen Y, Jiang G, Chen S, Guo Z, Yu X, Zhao C, Zhang H, Bao Q, Wen S, Tang D (2015) Mechanically exfoliated black phosphorus as a new saturable absorber for both Q-switching and mode-locking laser operation. Opt Express 23:12823–12833
26. Su Z, Yin J, Zhao X (2015) Terahertz dual-band metamaterial absorber based on graphene/MgF 2 multilayer structures. Opt Express 23:1679–1690
27. Qi Y, Zhang Y, Liu C, Zhang T, Zhang B, Wang L, Deng X, Bai Y, Wang X (2020) "A tunable terahertz metamaterial absorber composed of elliptical ring graphene arrays with refractive index sensing application". Results Phys 16:103012
28. Aslinezhad M (2020) "High sensitivity refractive index and temperature sensor based on semiconductor metamaterial perfect absorber in the terahertz band". Opt Commun 463:125411
29. Hashemi S, Faez R, Darvish G (2020) Computational study of spin caloritronics in a pristine and defective antimonene nanoribbon. Physica E Low Dimens Syst Nanostruct 120:114083
30. Harris DC, Johnson LF, Cambrea LR, Baldwin L, Baronowski M, Zelmon DE, Poston WB, Kunkel JD, Parish MV, Pascucci MR (2017) Refractive index of infrared-transparent polycrystalline alumina. Opt Eng 56:077103
31. Johnson PB, Christy R-W (1972) Optical constants of the noble metals. Phys Rev B 6:4370

Figures

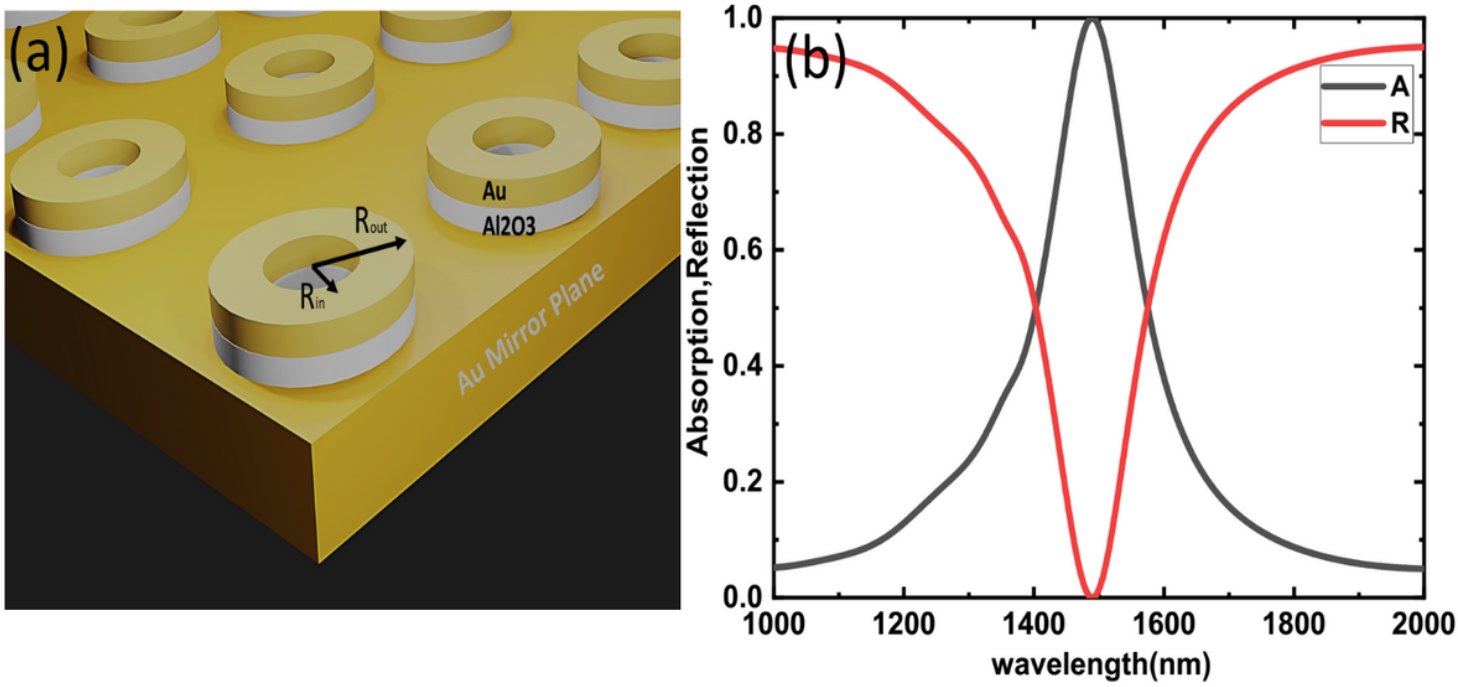

Figure 1

(a) The schematic diagram of the proposed metasurface device consisting of gold-alumina ring resonators on gold mirror backplane. (b) The absorption A and reflection R at normal incidence of the electromagnetic waves.

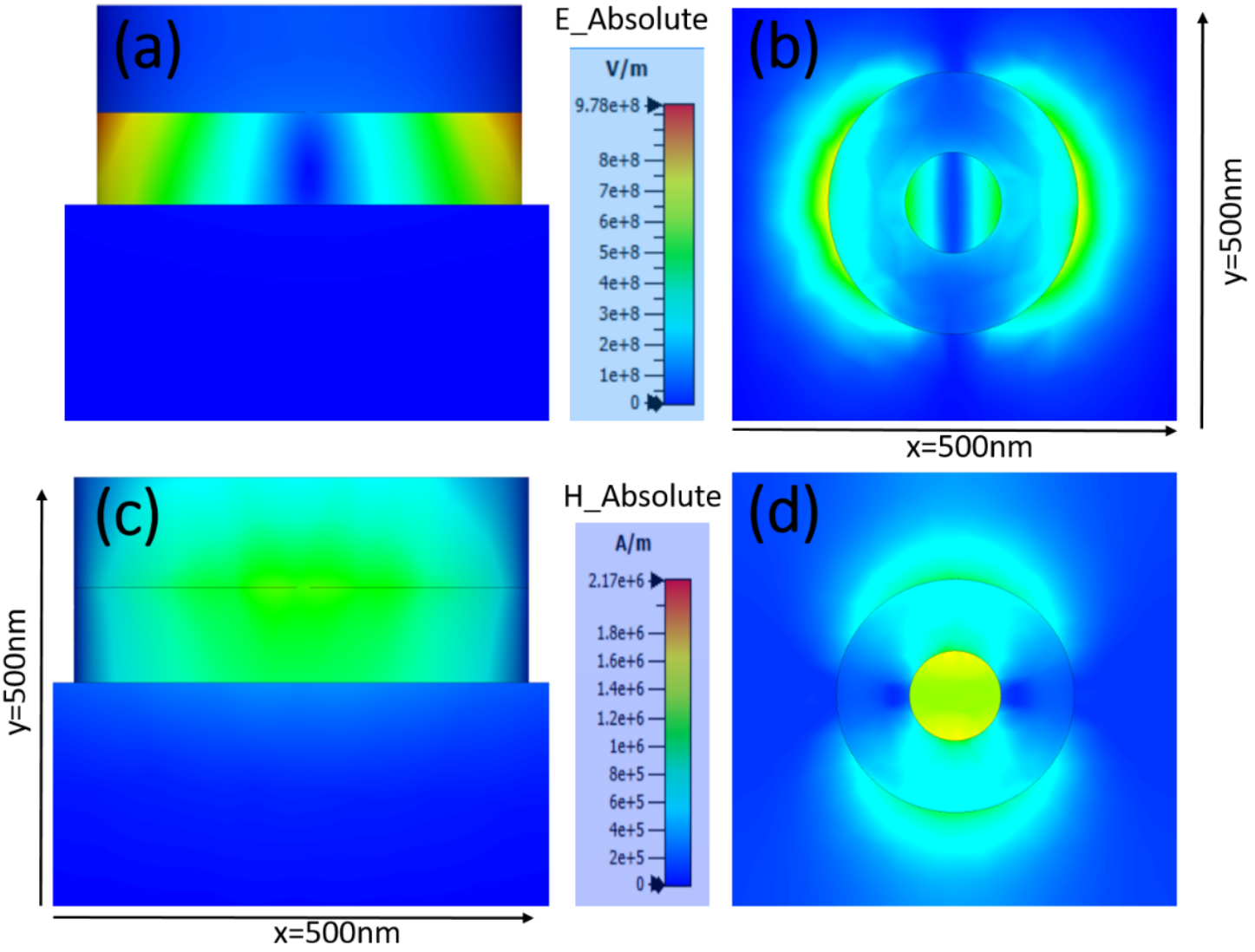

Figure 2

Electric and magnetic field distribution in both front and side view. (a,b) The absolute amplitude of electric field distribution at resonance peak 1490 nm while (c,d) the absolute value of H-field at resonance peak value 1490 nm of the absorption spectrum.

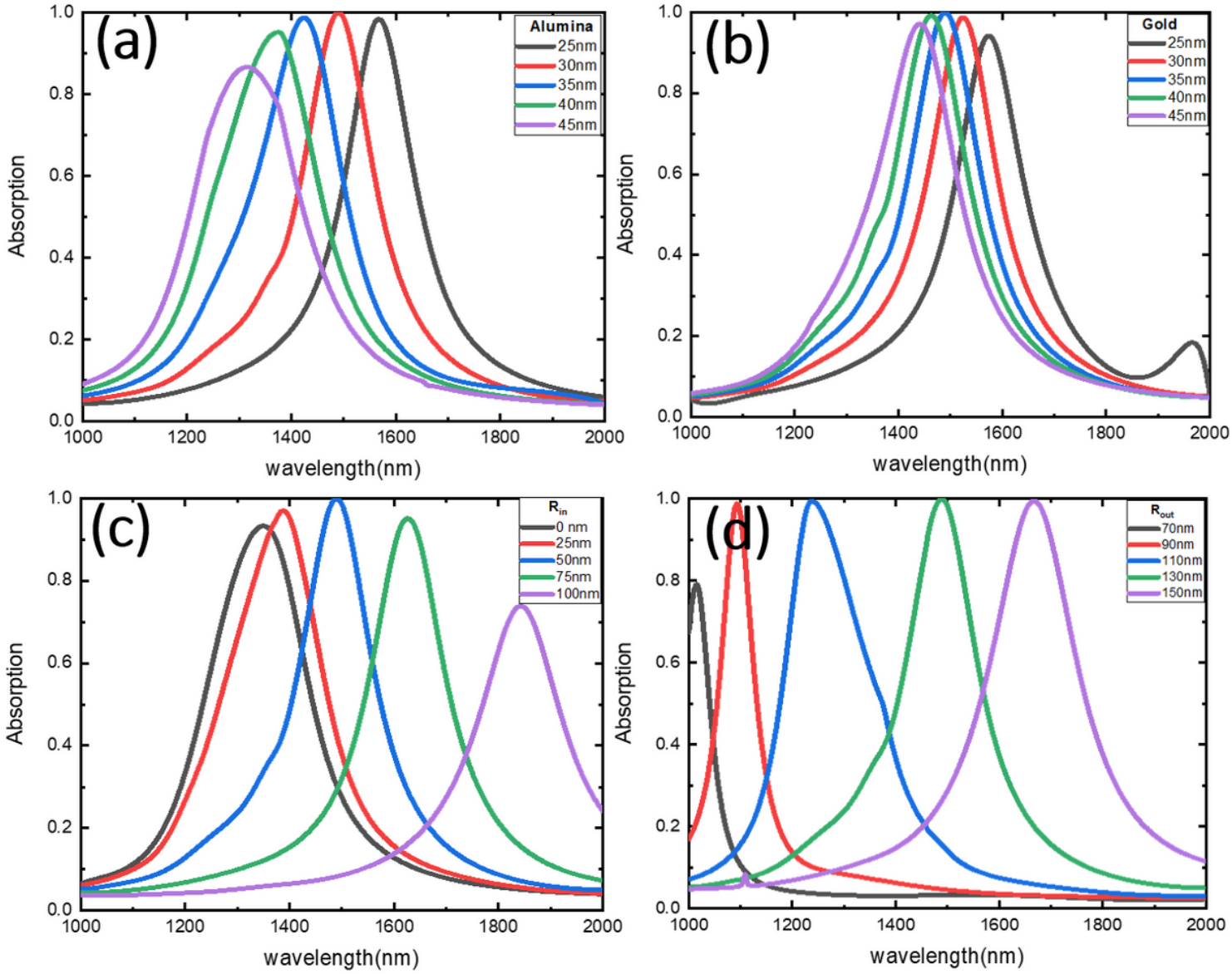

Figure 3

The device total absorption spectra at various dimensions of (a) Alumina disk with height h2 from 25 nm to 45 nm for fixed gold h1 35 nm. Similarly, (b) shows the effect of different gold values for fixed h2 alumina of 30 nm. The configuration was also evaluated for different values of (c)Inner R¬in and (d) Outer Rout radii at the resonators constant height.

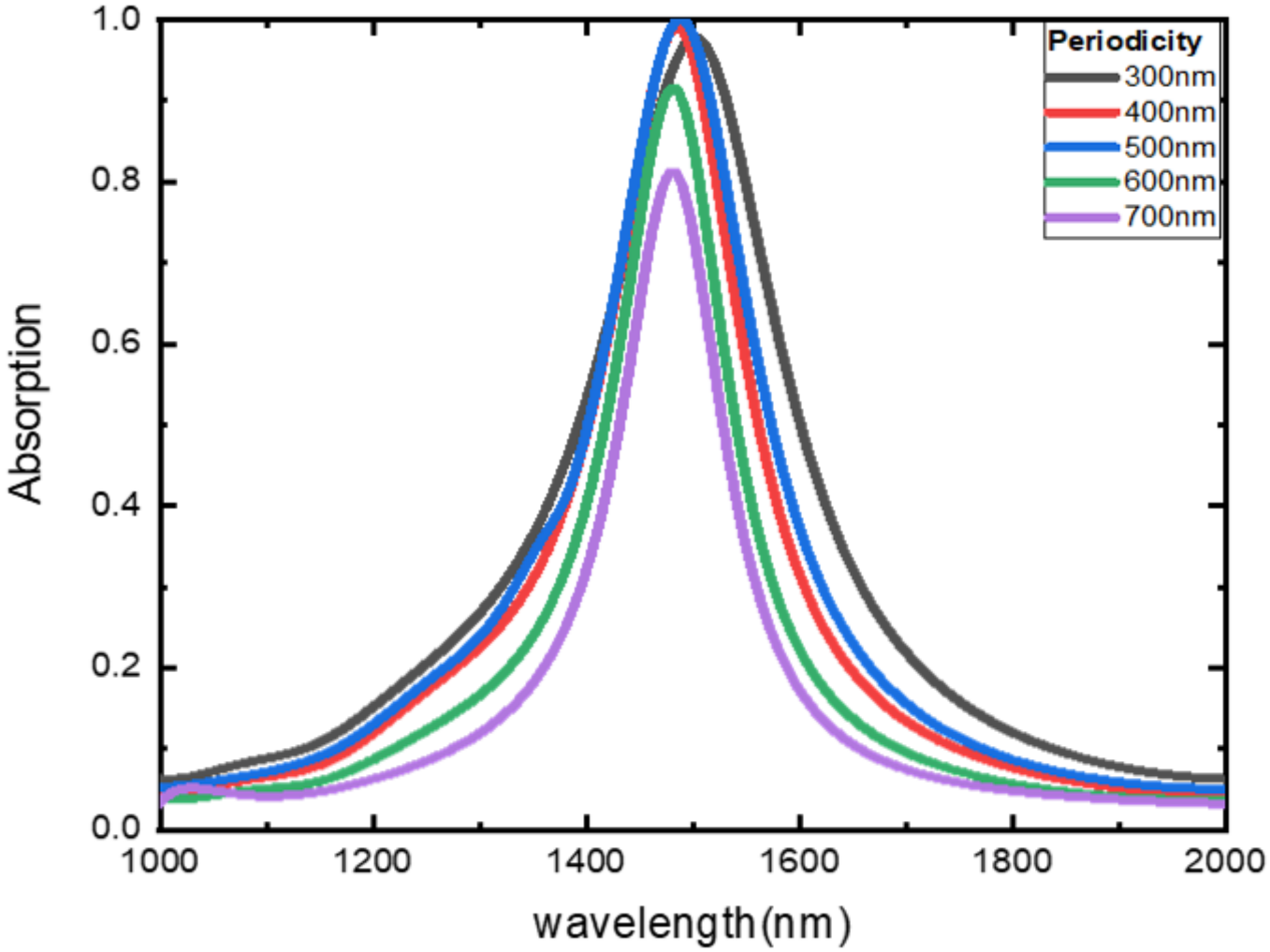

Figure 4

The absorption spectra at a different periodicity of the unit cell of the metasurface.

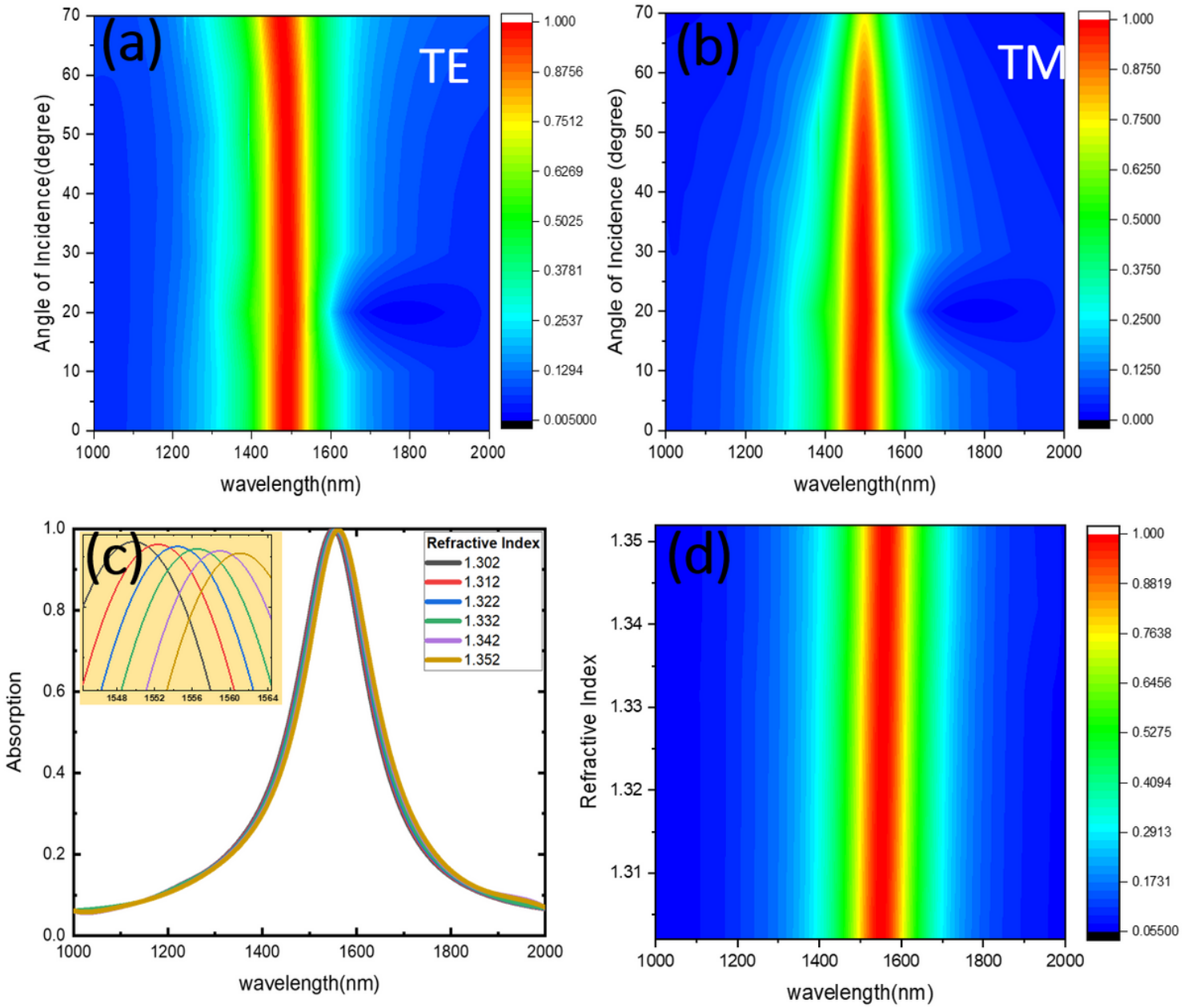

Figure 5

Absorption intensity and plasmon resonance position wavelength of the plasmonic absorber for both (a) TE and (b) TM polarization modes of the electromagnetic waves. (c) The proposed absorber's absorption spectra for sensing different refractive indices with an inset view of the resonance shift (d) the refractive index's contour plot versus the resonance wavelength.

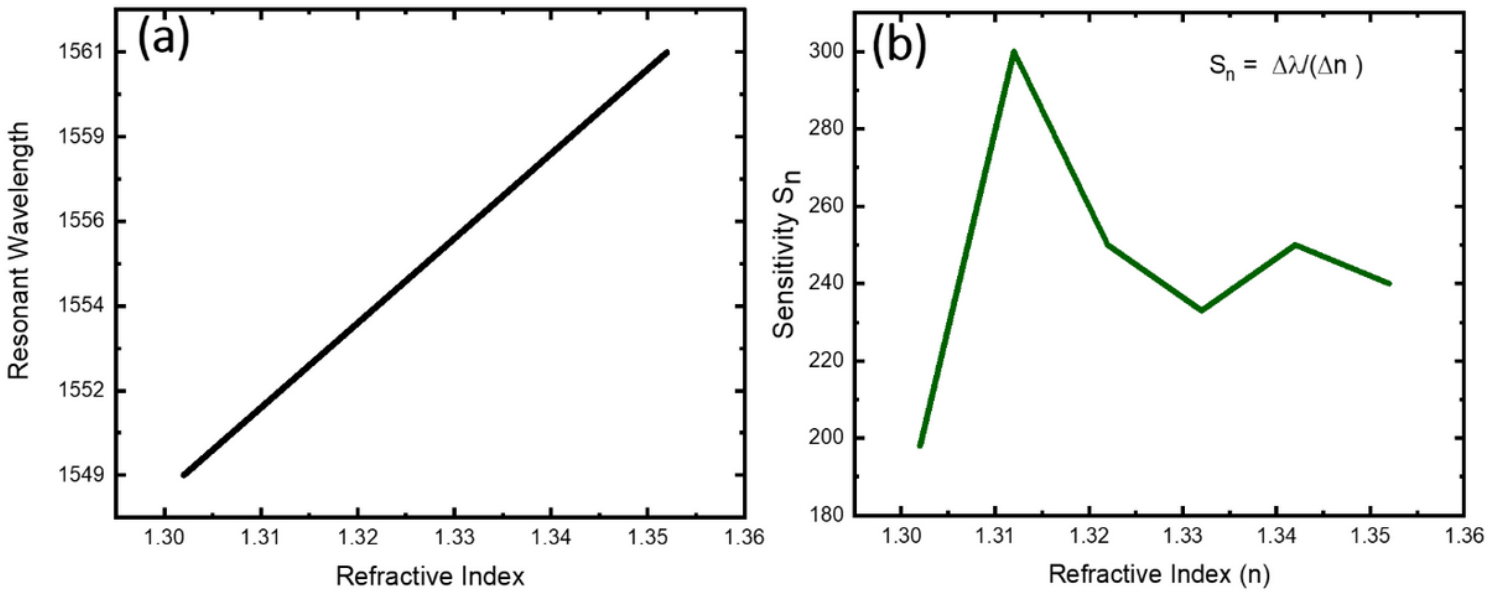

Figure 6

The resonance wavelength as a function of refractive index (a) wavelength shift versus the refractive index and (b) sensitivity of the device for the various analyst of refractive index having a range of 1.302-1.352.